
Article:
Yoshida, Kenta, Zhang, Xudong, Shimada, Yusuke et al. (7 more authors) (2019) Influence of gas environment and heating on atomic structures of platinum nanoparticle catalysts for proton-exchange membrane fuel cells. Nanotechnology. pp. 1-12. ISSN 0957-4484

https://doi.org/10.1088/1361-6528/aafe1e

APP Template V1.70 Article id: nanoaafe1e Typesetter: MPS Date received by MPS: 15/01/2019 PE: MAC006552 CE: LE:

IOP Publishing Nanotechnology

Nanotechnology **00** (2019) 000000 (11pp)

Influence of gas environment and heating on atomic structures of platinum nanoparticle catalysts for proton-exchange membrane fuel cells

Kenta Yoshida[1,2,3,8], Xudong Zhang[2], Yusuke Shimada[1], Yasuyoshi Nagai[1], Tomoki Hiroyama[2], Nobuo Tanaka[2,3], Leonardo Lari[4,5], Michael R Ward[4,5], Edward D Boyes[4,5,6] and Pratibha L Gai[4,5,7,8]

[1] International Research Center for Nuclear Materials Science, Institute for Materials Research, Tohoku University, Oarai, Ibaraki 311-1313, Japan
[2] Nanostructures Research Laboratory, Japan Fine Ceramics Center, Atsuta-ku, Nagoya, 456-8587, Japan
[3] Institute for Materials Research & IMass, Nagoya University, Chikusa-ku, Nagoya, 464-8603, Japan
[4] The York JEOL Nanocentre, University of York, Heslington, York, YO10 5BR, United Kingdom
[5] Departments of Physics, University of York, Heslington, York, YO10 5DD, United Kingdom
[6] Departments of Electronics, University of York, Heslington, York, YO10 5DD, United Kingdom
[7] Departments of Chemistry, University of York, Heslington, York, YO10 5DD, United Kingdom

E-mail: k_yoshida@imr.tohoku.ac.jp and pratibha.gai@york.ac.uk

Received 29 July 2018, revised 15 December 2018
Accepted for publication 14 January 2019
Published DD MM 2019

Abstract

Atomic-scale relaxations of platinum nanoparticles (Pt NPs) for fuel-cell catalysts are evaluated by spherical-aberration corrected environmental transmission electron microscopy (ETEM) under reference high-vacuum and N_2 atmospheres, and then under reactive H_2, CO and O_2 atmospheres, combined with *ex situ* durability test using an electrochemical half-cell. In high-vacuum, increasing roughness due to continuous relaxation of surface-adsorbed Pt atoms is quantified in real-space. Under H_2 and N_2 atmospheres at a critical partial pressure of 1×10^{-2} Pa the stability of the surface facets is for the first time found to be improved. The adsorption behaviour of CO molecules is investigated using experimentally measured Pt–Pt bond lengths on the topmost surface layer of Pt NPs. The deactivation of Pt NPs in the anode environment of a proton-exchange-membrane fuel-cell is demonstrated at the atomic-scale in the ETEM, and the transformation of NPs into disordered nanocluster is systematically quantified using the partial size distribution of Pt atomic clusters under controlled heating experiments at 423, 573 and 723 K.

Supplementary material for this article is available online

Keywords: environmental transmission electron microscopy, *in situ*, nanoparticle, surface, catalysts

SQ1 (Some figures may appear in colour only in the online journal)

1. Introduction

Platinum nanoparticles (Pt NPs) on conductive carbon balls play a critical role for proton-exchange-membrane fuel cells, and their stability is essential for fuel cells' oxidation–

[8] Authors to whom any correspondence should be addressed.

reduction processes [1, 2]. Pt NPs are also used as promising electrode catalysts for various fuel-cell systems to enhance the activity of electrochemical oxidation of CO and methanol [3, 4]. It is also known that Ru doping and oxide support choice can drastically improve the NPs' susceptibility for CO poisoning. Thus, the performance of such platinum–carbon (Pt/C) electrode catalysts has often been evaluated on the basis of the size distribution and coalescence behaviour of Pt NPs, the latter of which is responsible for a reduction in the active surface area and therefore catalysts activity. In addition, the surface atoms of Pt NPs under fuel-cell operating conditions are known to be dynamically relaxed during electrochemical reactions [5–8]. Such atomic relaxation has already been defined in real-space using structure-sensitive reactions such as cyclopropane hydrogenolysis [9].

Environmental transmission electron microscopy (ETEM) is a powerful tool for atomic-scale visualisation of Pt NPs heterogeneously dispersed for Pt/C electrode catalysts. Since our first development of atomic resolution-ETEM in 1997 [10] to directly visualise and analyse gas–solid reactions at the atomic-level, many researchers have used this tool for direct observation of various NP catalysts with nano- and atomic-level resolutions [11–14]. The surface structures of Pt NPs in vacuum, hydrogen (H_2), and oxygen (O_2) atmospheres have been evaluated by *ex situ* TEM and ETEM [15–18]. These reports have revealed the substantial complexity of the adsorption and desorption phenomena on the surface of Pt NPs at the nanoscale. Using the latest ETEM with atomic-scale resolution [19] and an advanced gas-mixing chamber [20] we have carried out *ex-situ* and *in situ* microscopy to investigate the dynamic behaviour of fuel-cell catalysts. This combination of analyses is very valuable to improve the understanding of the degradation mechanisms of Pt/C electrodes, i.e. platinum particle sintering, platinum dissolution, carbon support corrosion, corrosion by carbon monoxide and detachment from the carbon support. This knowledge is fundamental for improving the cathode robustness, which is one of the biggest challenges for its commercial use in fuel-cell vehicles.

In this paper, we report the first atomic-scale analyses of the surface structures of Pt NPs on amorphous carbon (Pt/C) in H_2, CO, N_2 and O_2 atmospheres and under high-vacuum; in addition to conventional *ex situ* TEM during the start-up endurance test [15]. This Pt/C material plays an important role as an electrode catalyst in fuel cells, which typically consist of bipolar plates, electrodes, a membrane separator and an electrode catalyst [21]. The stability of Pt/C under experimental conditions such as a controlled gas partial pressure and with active thermal heating are compared to elucidate the influence of adsorbed gases on the relaxation of the surface atoms of Pt NPs.

2. Experimental methods

Commercial Pt/C powders consisting of Pt NPs with an average diameter of 3 nm on Ketjen Black EC (25 w% Pt/Ketjen carbon black, TEC10EC25E, Tanaka Kikinzoku Kogyo K.K.) were used for *ex situ* TEM and for initial tests of atomic-scale resolution *in situ* ETEM.

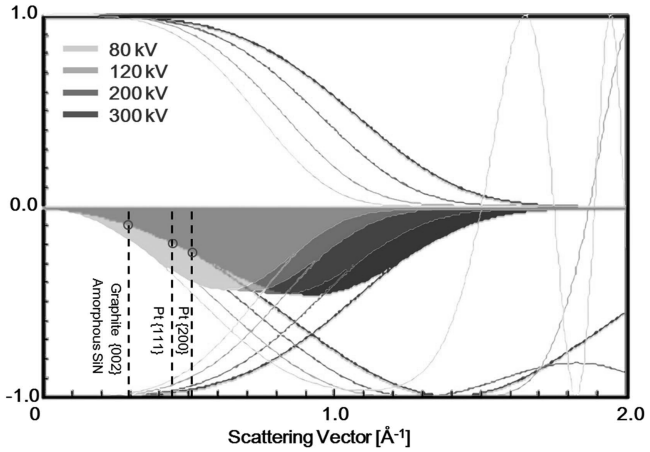

Figure 1. Contrast transfer functions of the spherical-aberration-corrected environmental transmission electron microscope used in this work at acceleration voltages of 80, 120, 200 and 300 kV and of a conventional transmission electron microscope with a spherical-aberration of 0.5 mm, operated at 200 kV.

The electrochemically active surface area (ECSA) of the Pt/C powders supported on a glassy carbon working electrode (ALS Glassy Carbon Electrode 6.0 × 3.0 mm, No002012, BAS Inc.) by Nafion (5% NafionTM Dispersion Solution, DE521CS, FUJIFILM Wako Pure Chemical Corporation) was evaluated by using a potentiometer (ALS Electrochemical Analyzer, 750E, BAS Inc.) during the start-up endurance test (lower threshold voltage of 400 mV, upper threshold voltage of 1100 mV, sweep rate of 500 mV s^{-1}). This is a standard test widely used by Japanese auto motor companies (FCCJ, No. III-2-2, 2009 NEDO). A pristine Pt/C powder and a powder after 40 000 cycles were individually prepared for *ex situ* TEM characterisation. For *in situ* ETEM observation the Pt/C powder samples were enclosed in an environmental cell using 5 nm thick SiN membranes as shown in figure S1 is available online at stacks.iop.org/NANO/0/000000/mmedia.

The model Pt/C catalysts were prepared by magnetron sputtering (Ar-Ion Sputter E-1030, Hitachi) on open cell MEMS-based environmental chips (E-chips, Protochips Inc.). The Ar-ion sputter deposition was carried out at room temperature and yielded a deposition rate of 0.05 nm s^{-1} at a pressure of 6.0 × 10^2 Pa. Details on the sample preparation are described in figure S2.

The total deposition time was 5 s, which resulted in a narrow size distribution of small Pt NPs on the amorphous carbon films.

A heating holder (Aduro, Protochips Inc.) was used for *in situ* heating of E-chips from RT to 1473 K. Size distributions of the NPs and Pt nanoclusters (NCs) were determined from spherical-aberration-corrected transmission electron microscopy (AC-TEM) images taken using an ETEM (Titan ETEM, FEI Company) equipped with a high-speed CCD camera (Orius SC200, Gatan Inc.).

Figure 1 gives the contrast transfer function (CTF) of the ETEM at acceleration voltages of 80, 120, 200 and 300 kV; these values were calculated using lens parameters such as spherical-aberration ($Cs = 500$ nm), objective lens defocus ($\Delta f = -20$ nm), energy spread ($\Delta E = 20$ nm) and fifth-order aberration ($Cc = 0.1$ mm).

During *in situ* ETEM imaging, the electron illumination has to pass through gas molecules, SiN membrane windows, and carbon supports with a possible deterioration of resolution. In order to achieve atomic-resolution of Pt NPs in these conditions we can adopt two approaches. One approach is to fine-tune the acceleration voltage of the AC-TEM. In fact, the Peak position of the CTF is shifted to higher frequencies by increasing the acceleration voltage (meaning better resolution), as shown in figure 1.

The highest acceleration voltage available in 2018 for AC-TEM is 300 keV. This provides a better information limit for the atomic-scale observation of the Pt NPs despite the poor contrast resulting from the conductive carbon supports with the lattice spacing of graphite (002), $d = 0.34$ nm (0.29 Å^{-1}). The 300 keV AC-TEM also minimises the contrast of gas molecules and the granular contrast due to the amorphous SiN window, but the carbon hexagon in conductive supports, and adsorbed molecules, are never visualised in the present imaging conditions. We used a 300 keV electron beam for visualising the atomic structures of Pt NPs in the subsequent experiments.

Another approach is to minimise scattering objects except for Pt NPs in the sample. This is the basic concept used for the present experiment using a model Pt/C sample. In order to remove the SiN windows and carbon supports, a diamond-like carbon (DLC) film of 3 nm thickness was synthesised from CH_4 and C_2H_2 gasses using a chemical vapour deposition method (SURFCOM 1400D, ACCRETECH Co.). The Size of Pt NPs and conductivity of DLC film was comparable to commercial Pt/C powders (Ketjen Black EC). *In situ* ETEM observation was performed in a gas environment with the lowest partial pressure achievable. The lowest partial pressure was obtained using H_2: this having a lower activation energy for absorption on Pt compared to CO and O_2.

Video-capture software (VisualDub, licensed under the GNU General Public License) was configured with an image size of 620 pixel × 480 pixel and a time resolution of 0.05 s. The Digital Micrograph (Gatan Inc.) program and Vesta software [22] were used to analyse the AC-TEM images of Pt NPs and for construction of the atomic model, respectively.

3. Results and discussion

3.1. Ex situ and in situ durability test of Pt NPs on conductive Ketjen carbon black

In order to verify the consistency of our results, our *in situ* durability test performed in the ETEM was directly compared with a conventional durability test in an electrochemical half-cell. Figure 2(a) shows cyclic voltammetry (CV) curves (range: 50–1100 mV, RHE, sweep rate: 50 mV s^{-1}) obtained from the present Pt/C powders before and after an electrochemical durability test. For CV measurement of ECSA, 0.1 mol l^{-1} of perchloric acid ($HClO_4$) was used as an electrolyte. Deactivation was observed in the start-up endurance test with initial voltage of 1.0 V for 30 s, lower threshold voltage of 1.0 V, upper threshold voltage of 1.5 V and sweep rate of 500 mV s^{-1}. The ECSA, which is defined by Pt electrical charge of 210 μC cm^{-2}, decreased by 45% from 88.2 to 48.5 m^2 g^{-1} during the 40 000 cycle electrochemical durability test over 32 h. The reasons for Pt/C ECSA performance degradation were investigated by *ex situ* TEM.

Figures 2(b) and (c) shows TEM images and particle size distributions before and after the electrochemical durability test. Table 1 summarises estimated diameters of the carbon ball, densities of the NPs and specific surface areas in real-space. It is worth mentioning that the specific surface areas always showed slightly larger values than ECSA in our research because of miss-count of a Pt surface covered by carbon and CO molecules. *Ex situ* TEM observations clarified that in the case of the Pt/C powder (Pt 25 w%, Ketjen EC) sample, NPs became larger and densities of NPTs increased, with coalescence of NPs and shrinkage of carbon support expected as the main causes of such morphology changes.

In order to study dynamically coalescence of NPs and shrinkage of the carbon support, *in situ* ETEM observations were performed. The Pt/C powders were closed in an environmental cell formed by two SiN membranes of 5 nm in thickness (as shown in figure S1) to prevent contamination of the microscope vacuum parts. In this ETEM study, we used a uniform local current density of 1.8×10^3 A cm^{-2} with the AC-ETEM operating at 300 kV.

Figures 3(a) and (b) show a strong influence of anodic hydrogen environment and cathodic oxygen environment respectively on the structural deactivation of Pt/C powders. The stability of atomic structures of the Pt/C powders in a non-reactive nitrogen environment is shown in figure 3(c). Supporting materials include dynamic ETEM movies obtained from three different regions from the same Pt/C powders dispersed on a common microscopic grid, corresponding to the same areas shown in figures 3(a)–(c).

We found that a few Pt NPs migrate rapidly in a hydrogen environment, in spite of all other NPs being pinned in position. For example, in figure 3(a) particle (i) migrated with an average migration speed of 6.90 nm s^{-1} during an *in situ* observation of 0.67 s. In contrast, the centre of gravity of particle (ii) in the same figure, showed relative stability below 0.28 nm s^{-1}, which is comparable to a standard thermal drift level of the ETEM system. The driving force for Pt NP migration in an oxygen environment can be attributed to the shrinkage of carbon supports by radical species and oxygen atoms produced by EB ionisation. Figure 4(b) and Movie SM3 show such a deactivation process under cathodic conditions. When the edge of the carbon support moves from the initial position (black dotted line at 3.13 s) to the shrunk position (white-dotted line after 3.75 s), it resulted in a considerable apparent movement of NPs. NPs (iii) and (iv) were respectively shifted in opposite directions. Our *in situ* ETEM

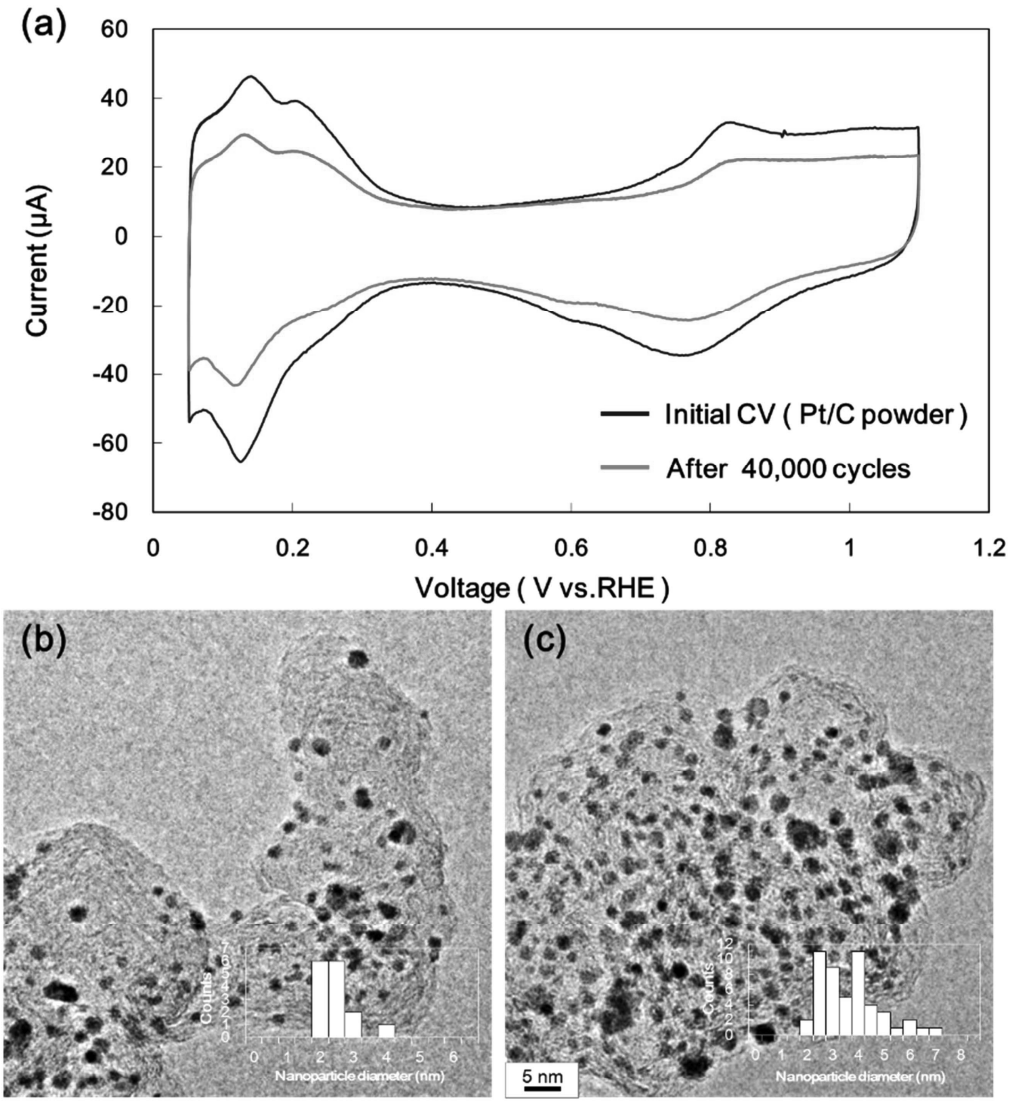

Figure 2. *Ex situ* TEM observation of Pt NPs on Ketjen Black EC during the start-up endurance test. CV curves before and after 40 000 cycles (a). Low-magnification TEM images and particle size distributions obtained from initial Pt/C powder (b) and after the electrochemical durability test (c).

Table 1. Changes of carbon ball diameter, density of Pt NPs and specific surface area during the start-up endurance test.

		Diameter of carbon ball (nm)	Density of nanoparticles (number nm^{-2})	Change ratio of density	Specific surface area ($m^2 g^{-1}$)	Change ration of specific surface area
Pt	Initial	34.7 ± 7.3	40.0×10^{-4}	1	109.92	1
	After 40 000 cycles	30.6 ± 5.8	129.9×10^{-4}	3.25	65.99	0.60

observations established reproducibly that the present sample are still stable in non-reactive N_2 gas environment with the same electron beam current density (1800–1900 A cm^{-2}) and illumination area (310–325 nm^2). We believe that the ETEM can be applied for selecting a suitable conductive carbon support from a number of candidates.

In the next section, we will tackle the atomic-scale relaxation mechanism of Pt NPs using a dedicated model structure.

3.2. Surface structures of Pt NPs under different pressures and various fuel-cell environments

Before evaluating the behaviour of the Pt NPs at high temperatures, we initially collected AC-TEM images at RT with the sample under various partial pressures of different gases for comparison purposes. The size distribution of the Pt NPs was evaluated on the basis of an average inter-nanoparticle distance of 1.5 ± 0.3 nm and an average nanoparticle size of 2.1 ± 0.4 nm. Although Boyes *et al* [23] previously reported

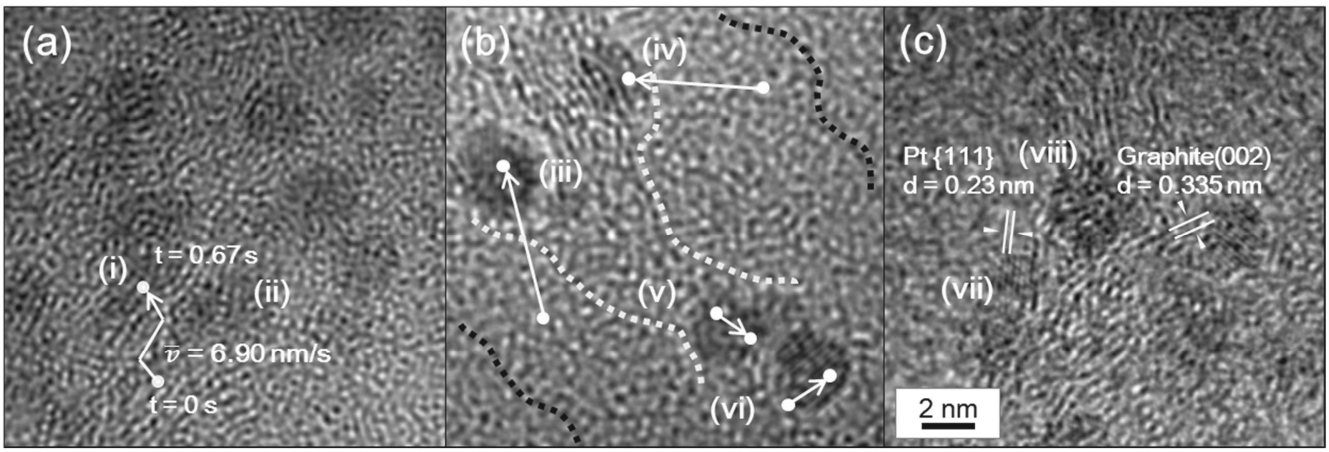

Figure 3. Migration of Pt nanoparticles in 0.1 Pa H_2 environment analysed from SAC images at 0.00 and 0.67 s (a), 0.1 Pa O2 environment, SAC image from movies at 3.13 and 3.75 s (b), 0.1Pa N_2 environment, SAC image from movies at 2.57 and 2.70 s (c).

a study of single atoms under gas environments, in the present atomic-scale ETEM study, we focus on the changes in the shape of NPs under different atmospheres and on their morphological changes during heating experiments.

Figure 4 shows the *in situ* ETEM observations of the Pt/C catalysts under different partial pressures of hydrogen gas at RT. We first focused on the morphological change of Pt NPs and enlarged the selected area to show the reconstruction shape. The surface structures of the Pt NPs were originally recorded in movie files using the ETEM and video-capture software. Selected area captured (SAC) images were then acquired by clipping individual frames from the dynamic movie files. Approximately 20–30 NPs were systematically analysed under each environmental condition. Additional SAC images are provided as figures S3–S10 in the supporting materials. All of the SAC images were compared along the ⟨110⟩ zone axis of face-centred-cubic (fcc) platinum (fcc-Pt; space group: *Fm*-3*m*).

Figure 4(a) is a SAC image obtained under high-vacuum conditions at 4.5×10^{-5} Pa. This image clarifies that the Pt NPs undergo continuous surface reconstruction and exhibit surface-adsorbed atoms, which are marked with white arrows in figure 4(a). In this figure the electron beam can function as a source of thermal heating induced by inelastic scattering, which enhances the atomic-scale-reconstruction of the Pt NPs. This enhanced reconstruction is attributed to local heating by electrons.

Single atoms (marked with circles in figure 4(a)) are also visible on the carbon support. We propose that surface-adsorbed atoms continuously move on the surface of Pt NPs, thus increasing their roughness [24]. Yoshida *et al* [25] and Boyes *et al* [23] have previously observed Ostwald ripening of Pt single atoms. Ostwald ripening of single atoms is often considered a specific pathway for atoms to detach from one nanoparticle and attach to another nanoparticle [23, 26]. Here, we observed at least a continuous shift of adsorbed surface atoms on the NPs; these adsorbed atoms never stabilised because of electron beam effects under the high-vacuum ETEM conditions. We then carefully increased the H_2 partial pressure to introduce additional gas molecules which directly contributed to the stabilisation of the surface structure.

Figures 4(b)–(h) shows SAC images with the sample under different partial pressures of H_2 ranging from 1×10^{-4} to 1×10^{2} Pa. We observed that the continuous surface reconstruction of Pt NPs was dominant under low-pressure H_2 atmospheres (figures 4(b), (c)), which is similar to high-vacuum conditions (figure 4(a)). Crystalline facets of the Pt NPs suddenly appeared under H_2 partial pressures greater than 1×10^{-2} Pa, as shown in figures 4(d)–(h). The atomic structures of the Pt NPs were clearly changed by H_2 gas introduced at different partial pressures. In higher pressure H_2 environments, above 1 Pa in figures 4(d)–(h), no adsorbed atoms on the Pt NP surfaces or single atoms on the amorphous carbon film were observed. A large number of H_2 gas molecules were expected to interact physically and/or chemically on the Pt surface [27]. The stable shape of Pt NPs in such a high H_2-partial-pressure environment was reasonable to be defined as the same as the Wulff shape obtained by minimising the surface free energy [28] in the limited two-dimensional projection of the TEM imaging. The surface energy of atomic planes of fcc-Pt NPs follows the order $\{111\}_{Pt} < \{100\}_{Pt} < \{110\}_{Pt}$, as reported by Skriver *et al* [29]. With higher-partial-pressure H_2 atmospheres, a greater proportion of {111} and {200} planes would be expected for faceted Pt NPs.

To define the atomic-scale relaxation of Pt NPs during fuel-cell reactions, we conducted second ETEM observations. The influences of the adsorbates on the structure of the Pt NPs were visualised. The ambient atmosphere is known to affect a substantial fraction of atoms on the surface when the NPs are smaller than 10 nm [30, 31]. Notably, the average size of Pt NPs in fuel cells is now reaching 3 nm or smaller.

Figures 5(a)–(d) shows AC-TEM images of the reconstructed surface of Pt NPs in H_2, CO_2, N_2 and O_2 environments, respectively, at a pressure of 1×10^{-2} Pa. Figures 3(a) and 5(c) present AC-TEM images which indicate that the Pt atoms on the topmost surface layer formed a hexagonal lattice without adsorbed atoms. Few individual Pt atoms were observed on the carbon film in H_2 and N_2

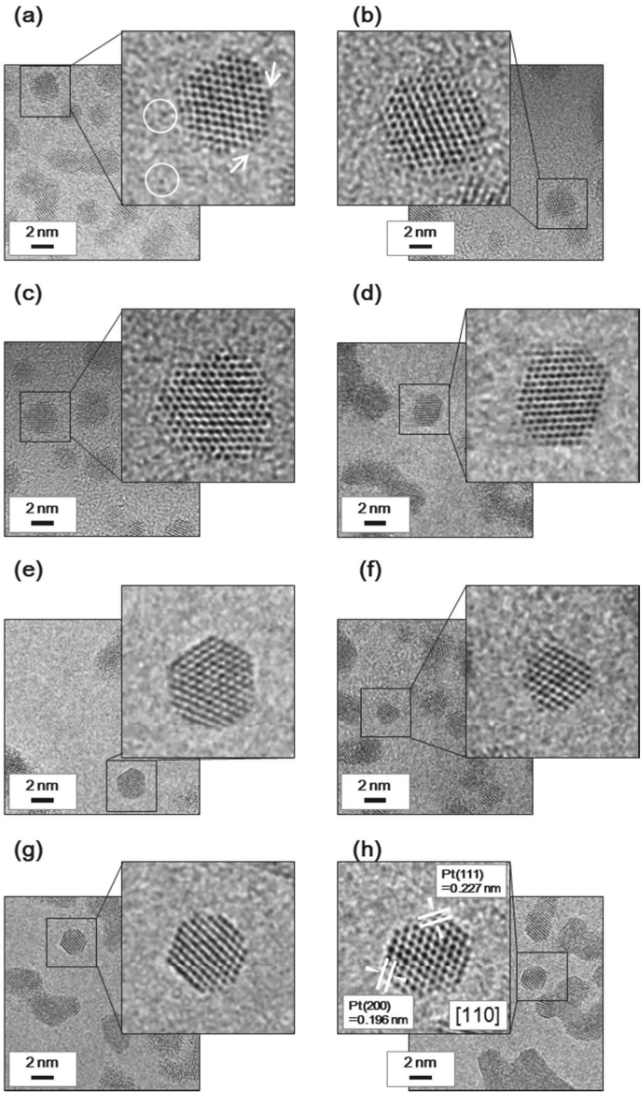

Figure 4. Partial-pressure dependence of the Pt surface structure. A series of selected area captured (SAC) images were collected with the sample under a high-vacuum of 4.5×10^{-5} Pa (a) and under H_2 atmospheres of 1×10^{-4} Pa (b), 1×10^{-3} Pa (c), 1×10^{-2} Pa (d), 1×10^{-1} Pa (e), 1 Pa (f), 10 Pa (g) and 1×10^{2} Pa (h). The arrows mark surface-adsorbed atoms, and the circles indicate single atoms on amorphous carbon films.

atmospheres of 1×10^{-2} Pa. In figure 5, as we expected, the Pt NPs were stabilised by H_2 or N_2 molecules at a high-partial pressure ($\geqslant 10^{-2}$ Pa), as also demonstrated in figure S11 in the supporting material. Faceted Pt NPs with distinct edges are a key feature for clarifying the stabilising effect by reducing or non-reactive gas molecules. The obviously round (less faceted) shape of Pt NPs in CO and O_2 atmospheres of 1×10^{-2} Pa are shown in figures 5(b) and (d).

Although a TEM micrograph gives only the 2D projection along the Pt [110] direction, we attempted to evaluate the average distance between adjoining Pt atomic columns on the (200) planes shown in the enlarged AC-TEM images, assuming that the CTF of the spherical-AC-ETEM could image the strain along the fcc-Pt ⟨100⟩ direction. Strain analysis of Au NPs along fcc-Au ⟨100⟩ direction has been reported by López-Haro *et al* [32]. The measuring error of the strain analysis using the geometrical phase analysis is below 0.01% of reference lattice distances [33]. Under the hypothesis that differences in lattice strain caused by adsorbed H_2, CO, N_2 and O_2 molecules are unique, a measurement of the nanoparticle strain will give us direct information on the NPs interaction with the gas environment. The measured maximum distances between adjoining atomic columns on the {200} planes of specimens under H_2, CO, N_2 and O_2 atmospheres at a pressure of 1×10^{-2} Pa were calculated as strain parallel to the interface (ε_{xx}) from the strain maps for the whole particles, and are summarised in table 2.

The deviations in the {200} plane of samples under O_2 and CO atmospheres are larger than those of samples under N_2 and H_2 atmospheres, and the formation of different shapes resulted from the different reaction gases. The results also suggest that surface layers of Pt NPs were composed of Pt lattice atoms in H_2 and N_2 atmospheres, without significant adsorption of gas molecules under the conditions employed.

The greater distance between the adjoining surface atomic columns improves the stability of the surface-adsorbed atoms on the Pt NPs. This result suggests that O_2 and CO molecules easily adsorb onto the Pt {200} planes.

In the present ETEM observations, the adsorption of O_2 or CO molecules onto the Pt surface appeared to enhance the surface reconstruction and to transform the NPs to a round shape. Because the literature contains numerous discussions on the influences of O_2 gas molecules on Pt surfaces, here we focus on CO molecules adsorbed onto the surface layers [6, 24]. The basic concept explaining the round shape of Pt NPs in a CO atmosphere is briefly described in figure 6, to understand the atomic-scale mechanism of CO poisoning of the Pt/C catalysts. We propose that Pt surface-adsorbed atoms were observed because of heterogeneous adsorption of CO molecules onto top sites. The movement of surface-adsorbed atoms became difficult because Pt–Pt bonds and Pt–CO bonds randomly existed on the surface layers. CO molecules on the front or the back of the surface-adsorbed atoms were not visible. The distances between adjoining surface-adsorbed atoms could shift with lattice atoms when some CO molecules adsorbed around them. This consideration can explain experimental results obtained in CO environments. Only in CO atmosphere of high-partial-pressure ($\geqslant 10^{-2}$ Pa), many stable surface-adsorbed atoms were observed on Pt NPs, but no ad-atoms on the carbon support film were visible.

We have used a truncated-octahedral shape, which is the most stable structure for Pt NPs for modelling [34, 35]. The concept of strained surface atomic layers, which could enhance activity for CO oxidation in the case of ultra-small decahedral gold NPs [36, 37], was expanded to similar fcc-Pt NPs.

The strained surface atomic layer was composed of CO molecules and Pt surface-adsorbed atoms (upper figure 6(a)) under CO atmosphere. Distances (L_1 or L_2 in figure 6(a)) between adjoining surface-adsorbed atoms could shift when some CO molecules adsorbed around them. The amount of surface-adsorbed atoms increased the roughness of Pt NPs,

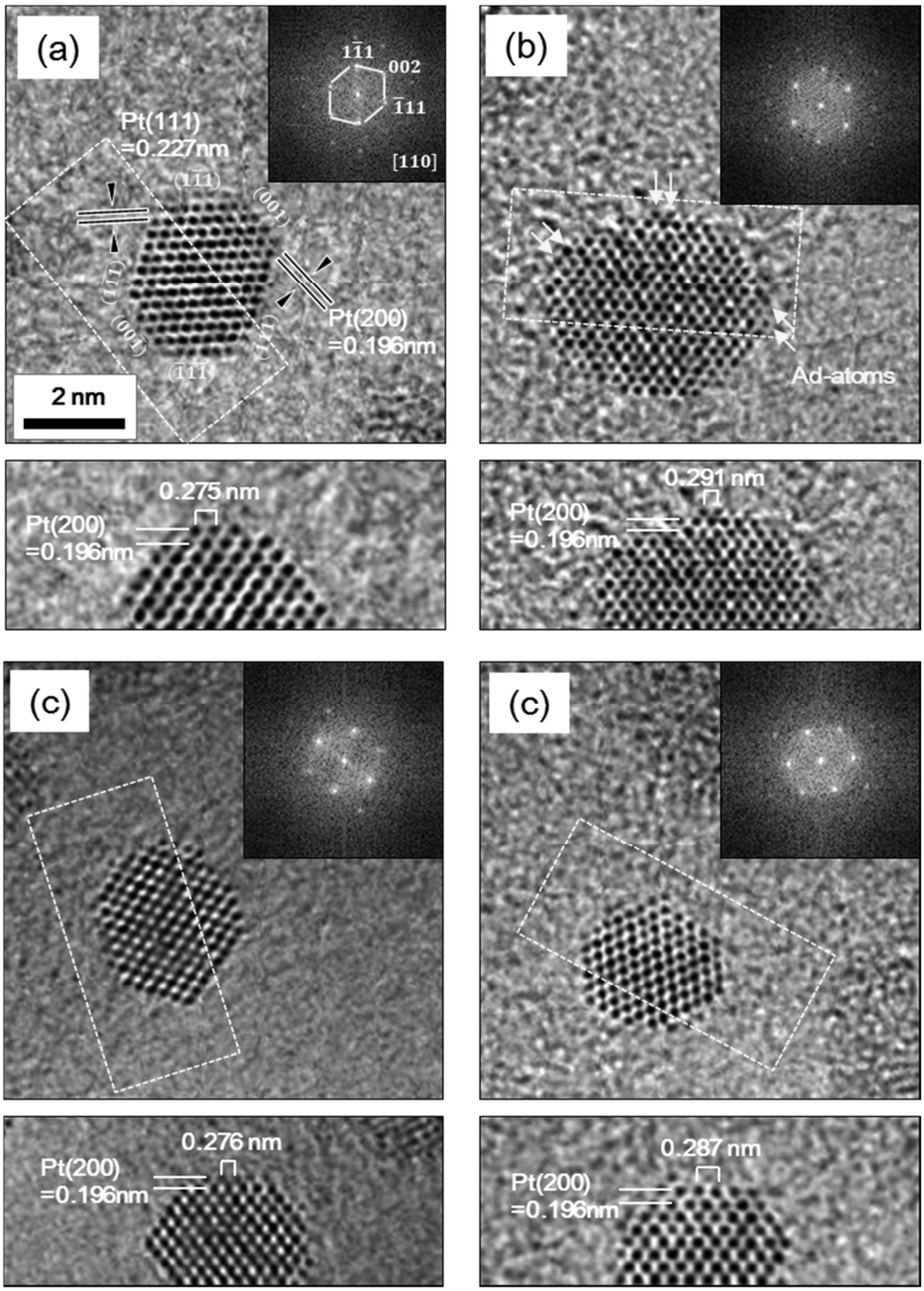

Figure 5. SAC images of the Pt/C catalysts under a H_2 atmosphere of 1×10^{-2} Pa (a), CO atmosphere of 1×10^{-2} Pa (b), N_2 atmosphere of 1×10^{-2} Pa (c) and O_2 atmosphere of 1×10^{-2} Pa (d) at RT; their fast Fourier transform patterns are shown as insets. The reconstructed surfaces of Pt NPs are enlarged.

which was reconstructed with the image along the [110] axis (figure 6(b)). Figure 6(c) shows the reconstruction of the Pt NPs in a high-partial-pressure of N_2 atmosphere. This figure indicates that reconstruction of the Pt NPs to form faceted surfaces, minimising the surface energy contribution of subsequently incorporated Pt atoms. Because the surfaces of the Pt {111} and {100} planes are more stable than those of the other planes [38], the competition between surface energies could control the shape [39]. A study on CO molecules adsorbed onto Au NPs provides reference information about the morphology change [40]. In summary, the surface layers of Pt NPs in a 99.95% pure CO environment was successfully visualised to elucidate the deactivation process of the Pt/C catalysts and the corresponding structural model was presented. We confirmed that CO molecules are invisible on Pt NPs even when we use a perfect model sample and a lower partial pressure for atomic-scale visualisation. It was also indicated that surface layer of Pt NPs and its strain were

Table 2. Distances between adjoining atomic columns on the {200} plane of Pt.

Gas environment	Distance between adjoining atomic columns on {200} plane (nm)	Deviation with the distance in vacuum
H_2	0.275	0.72%
O_2	0.287	3.61%
N_2	0.276	0.36%
CO	0.291	5.05%

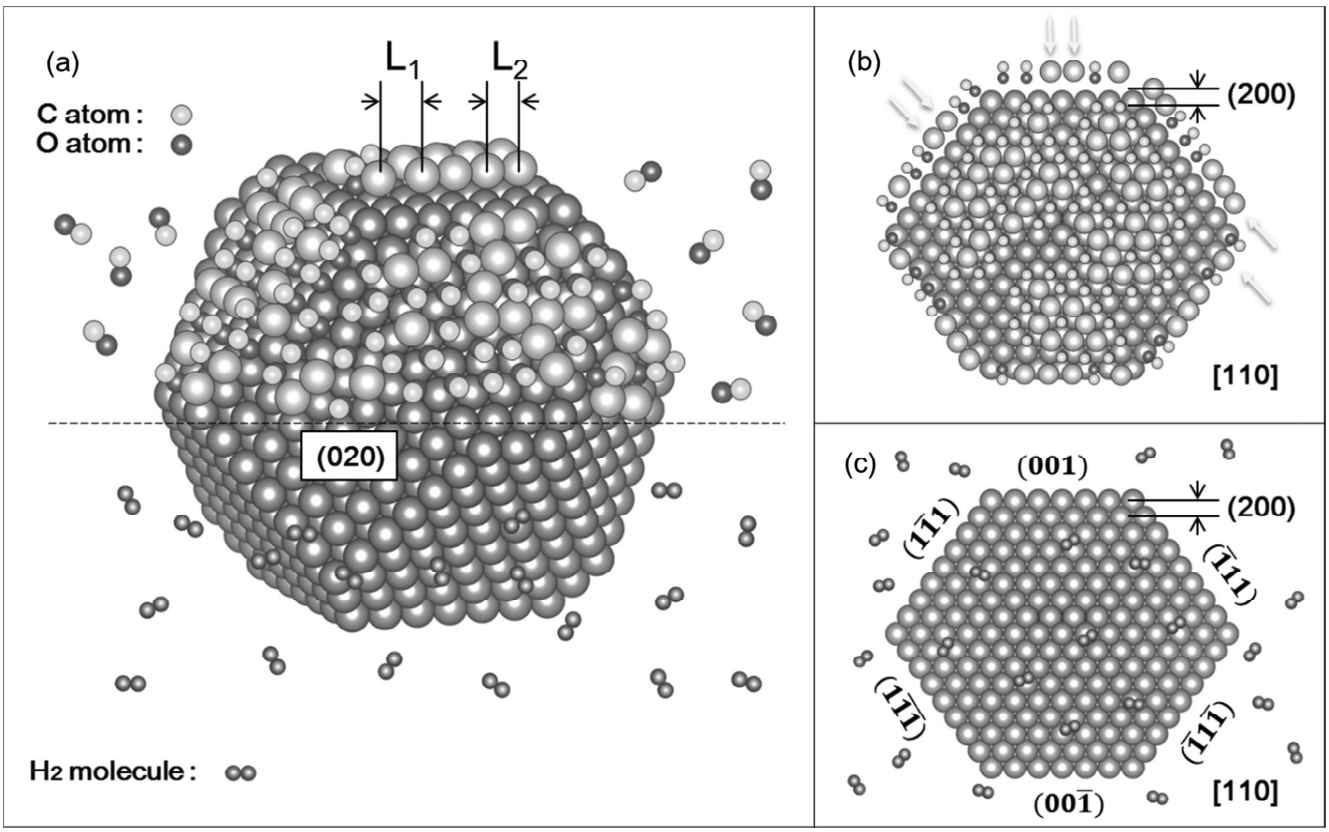

Figure 6. Structural models of Pt NPs with a truncated-octahedral shape (a) and along the [110] axis (b) and (c) in an atmosphere of high-partial-pressure H_2 or N_2 ($\geqslant 1 \times 10^{-2}$ Pa). Pt atoms, grey balls; Pt surface-adsorbed atoms, orange balls; C atoms, bright-green balls; O atoms, dark-green balls; H atoms, blue balls.

strongly affected by each gas environment. We believe such strain analysis will contribute to a deeper understanding of the CO poisoning of the Pt/C in the future.

3.3. In situ heating observation of Pt/C catalysts in a H_2 environment at 423, 573 and 723 K

In the final part of the present *in situ* experiment, we demonstrate the strong potential of the atomic resolution-ETEM for the fundamental study of size effects on NP catalysts. The model sample consisting of Pt NPs and DLC carbon film enables us to anneal NPs in a flowing H_2 gas environment (anode environment) and other gases environments in real-space and in atomic-scale in spite of electrochemical evaluation of ECSA. Although the ETEM evaluation needs a special *in situ* microscope and produces some difficulties in addition to the conventional electrochemical evaluation of the Pt/C catalysts, we should share the structural changes of very small (nm) Pt NPs discovered by the present *in situ* heating observation of Pt/C catalysts in a H_2 environment, which are too big to ignore.

We compared the growth of Pt NCs and NPs by measuring the average sizes after annealing the samples at 423, 573 and 723 K for 1 h in a H_2 atmosphere of 1×10^{-2} Pa. Significant evolution of Pt/C catalysts exposed to different thermal energies was achieved, as shown in figures 7(a)–(c). Movie files obtained from Pt/C catalysts at 423, 573 and 723 K are available in supporting materials. NCs and NPs were carefully distinguished by the subtraction of potential images in dynamical AC-TEM as shown in figure S12. In this study, the size distributions between the Pt NPs and NCs obtained at different temperatures of the ceramic heater on the E-chip were quantified to obtain new insights into the migration and coalescence processes of Pt NPs on conductive carbon supports. The average sizes of Pt NCs were 1.63 ± 0.15, 2.06 ± 0.09 and 4.35 ± 1.34 nm at 423, 573 and 723 K, respectively. By contrast, the average sizes of Pt

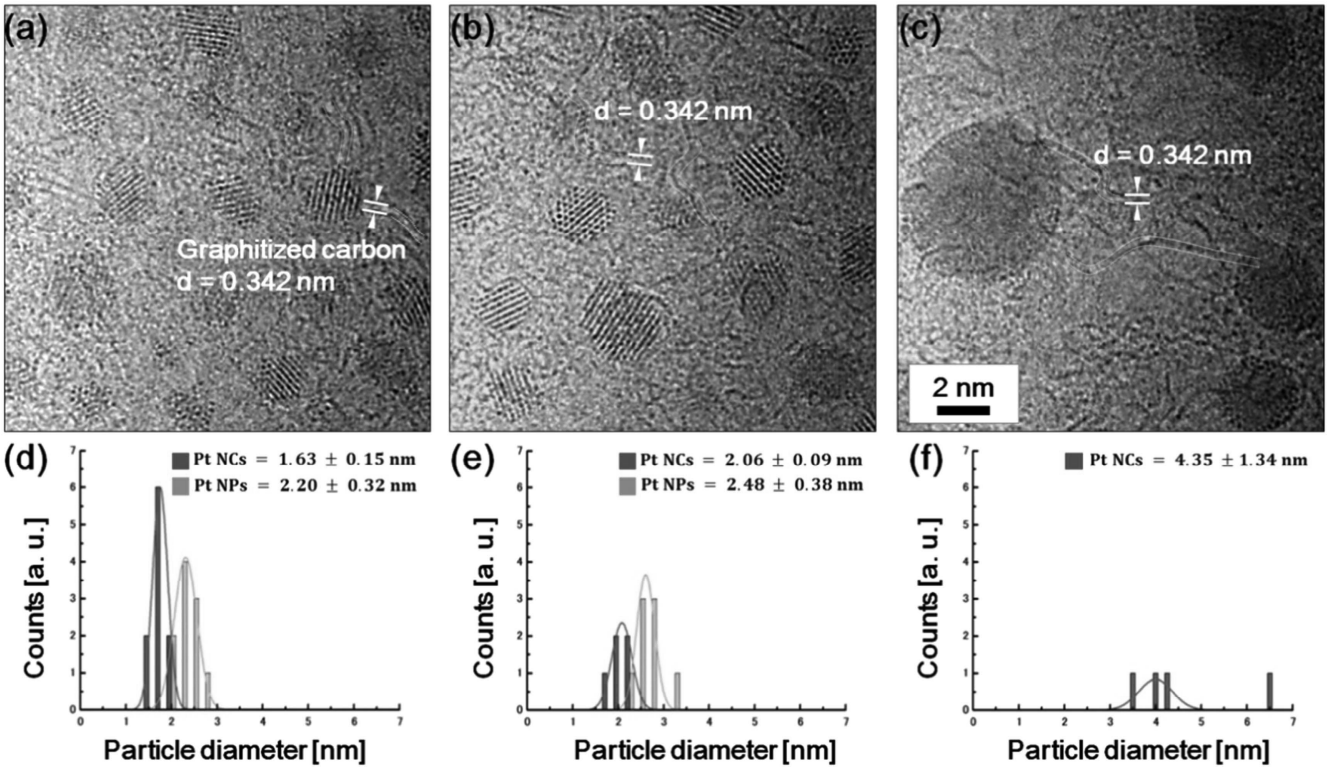

Figure 7. High-resolution AC-TEM images and the corresponding particle-diameter histograms of Pt NCs and NPs on a carbon film under a H_2 atmosphere of 10^{-2} Pa after 1 h heating at 423 K (a), (d), 573 K (b), (e), and 723 K (c), (f). White-dotted lines in (a)–(c) show the graphitised carbons.

NPs were 2.20 ± 0.32 and 2.48 ± 0.38 nm at 423 and 573 K, respectively, and Pt NCs with lattice atoms were not observed at a high temperature of 723 K. The size of the NPs was measured to obtain insights into the structure and properties of these NPs after *in situ* heating in the gas atmospheres. The measurements revealed that the size thresholds between Pt NCs and NPs on amorphous carbon were influenced by *in situ* heating, as indicated by the average sizes of the Pt NCs and NPs simultaneously increasing at the corresponding temperatures. Graphitised carbon is marked with white-dotted lines in figures 7(a)–(c). Such graphitisation was not observed at RT. These results indicate that all atoms composing Pt NCs —both those at the surface and those in the interior—interact with each other and that stable structures are dominated by the size and thermal energy. The *in situ* heating observation in atomic-resolution ETEM could visualise a pre-crystalline unstable structure, which was discovered in the Pt/C catalysts annealed under a flowing H_2 environment as a first step of real-space visualisation of important empirical rules such as the quantum size effect and the trapping sites on conductive carbons in the present Pt/C electrode fuel-cell catalysts.

4. Conclusions

In this study, we have described the effects of gas molecules on Pt NPs, directly visualised and analysed by *in situ* ETEM in addition to *ex situ* durability test using an electrochemical half-cell. The partial-pressure dependence of the Pt surface atomic structure of Pt NPs supported on amorphous carbon films was studied in reactive gas atmospheres under both the e-beam and controlled heating conditions. In high-vacuum the irradiation with 300 keV electrons led to the promotion of Pt single atoms on the NP surface and on the amorphous carbon film. The formation of facets of Pt NPs was observed under atmospheres of a relatively high H_2 partial pressure ($>1 \times 10^{-2}$ Pa) where the gas molecules directly contributed to the stabilisation of the surface structure.

We propose that the surface layer of Pt/C is composed of CO molecules and Pt surface-adsorbed atoms. In addition, Pt NCs and NPs are first distinguished by high-resolution AC-TEM images upon thermal heating in a flowing H_2 environment. These measurements are useful in understanding how partial pressure and thermal energy affect the surface atomic structure and coalescence process of Pt NPs. Our dynamic *in situ* experimental findings reveal that atomic-level structural changes of the Pt NPs at elevated temperatures modify the deactivation process of Pt/C electrode catalysts under fuel-cell conditions and generally improve NP stability.

Acknowledgments

This work was partly supported by a Grant-in-Aid for Young Scientific Researchers (A) (Nos. 16H02446 and 16H05966) from the Japan Society for the Promotion of Science (JSPS) Japan. The SEM and TEM usage fees were supported by a grant from Institute of Advanced Research, Nagoya

University. The authors thank Dr Alexander N Bright at Thermo Fisher Scientific for installing the aberration-corrected environmental transmission electron microscope for fuel-cell studies. Mr T Ikai, Mr H Kato and Mr T Nagami from TOYOTA MOTOR CORPORATION are gratefully thanked for discussions on electrochemical endurance tests. PLG and EDB thank the EPSRC (UK) for the research grant EP/J0118058/1.

ORCID iDs

Kenta Yoshida https://orcid.org/0000-0001-6907-6933
Yusuke Shimada https://orcid.org/0000-0003-0348-2765

References

[1] Asoro M A, Kovar D, Shao-Horn Y, Allard L F and Ferreira P J 2010 Coalescence and sintering of Pt nanoparticles: *in situ* observation by aberration-corrected HAADF STEM *Nanotechnology* **21** 025701
[2] Ferreira P J, la O' G J, Shao-Horn Y, Morgan D, Makharia R, Kocha S and Gasteiger H A 2005 Instability of Pt/C electrocatalysts in proton exchange membrane fuel cells *J. Electrochem. Soc.* **152** A2256
[3] Antolini E and Perez J 2011 The renaissance of unsupported nanostructured catalysts for low-temperature fuel cells: from the size to the shape of metal nanostructures *J. Mater. Sci.* **46** 4435
[4] Lee S W, Chen S O, Sheng W C, Yabuuchi N, Kim Y T, Mitani T, Vescovo E and Shao-Horn Y 2009 Roles of surface steps on Pt nanoparticles in electro-oxidation of carbon monoxide and methanol *J. Am. Chem. Soc.* **131** 15669
[5] Kamino T *et al* 2005 Development of a gas injection/specimen heating holder for use with transmission electron microscope *J. Electron Microsc.* **54** 497
[6] Yaguchi T, Suzuki M, Watabe A, Nagakubo Y, Ueda K and Kamino T 2011 Development of a high temperature-atmospheric pressure environmental cell for high-resolution TEM *J. Electron Microsc.* **60** 217
[7] Yoshida K, Arai S, Sasaki Y and Tanaka N 2015 Catalytic oxidation of carbon nanotubes with noble metal nanoparticles *Micron* **76** 19
[8] Yoshida K, Arai S, Sasaki Y and Tanaka N 2016 Catalytic behavior of noble metal nanoparticles for the hydrogenation and oxidation of multiwalled carbon nanotubes *Microscopy* **65** 309
[9] Zhang J Z, Hongsirikarn K and Goodwin J G Jr 2011 Effect and siting of Nafion® in a Pt/C proton exchange membrane fuel cell catalyst *J. Power Sources* **196** 7957
[10] Boyes E D and Gai P L 1997 Environmental high resolution electron microscopy and applications to chemical science *Ultramicroscopy* **67** 219
[11] Topsoe H 2003 Developments in operand studies and *in situ* characterization of heterogeneous catalysts *J. Catal.* **216** 155
[12] Thomasa J M and Gai P L 2004 Electron microscopy and the materials chemistry of solid catalysts *Adv. Catal.* **48** 171
[13] Crozier P A, Wang R and Sharma R 2008 *In situ* TEM studies of dynamic changes in cerium-based oxides nanoparticles during redox process *Ultramicroscopy* **108** 1432
[14] Hansen P L, Helveg S and Datye A K 2006 Atomic-scale imaging of supported metal nanocluster catalysts in the working state *Adv. Catal.* **50** 77
[15] Meier J C, Galeano C, Katsounaros L, Topalov A A, Kostka A, Schüth F and Mayrhofer J J 2012 Degradation mechanisms of Pt/C fuel cell catalysts under simulated start–stop conditions *ACS Catal.* **2** 832
[16] Bădescu Ş C, Jacobi K, Wang Y, Bedürftig K, Ertl G, Salo P, Ala-Nissila T and Ying S C 2003 Vibrational states of a H monolayer on the Pt (111) surface *Phys. Rev.* B **68** 205401
[17] Poelsema B, Lenz K and Comsa G 2010 The dissociative adsorption of hydrogen on defect-'free' Pt(111) *J. Phys.: Condens. Matter* **22** 304006
[18] Niet M J, Dunnen A, Juurlink L B and Koper M T 2010 The influence of step geometry on the desorption characteristics of O_2, D_2, and H_2O from stepped Pt surfaces *J. Chem. Phys.* **132** 174705
[19] Yoshida K, Tominaga T, Hanatani T, Tagami A, Sasaki Y, Yamasaki J, Saitoh K and Tanaka N 2013 Key factors for the dynamic ETEM observation of single atoms *Microscopy* **62** 571
[20] Yoshida K, Bright A N, Ward M R, Lari L, Zhang X, Hiroyama T, Boyes E D and Gai P L 2014 Dynamic wet-ETEM observation of Pt/C electrode catalysts in a moisturized cathode atmosphere *Nanotechnology* **25** 425702
[21] Yuan F and Ryu H 2004 The synthesis, characterization, and performance of carbon nanotubes and carbon nanofibres with controlled size and morphology as a catalyst support material for a polymer electrolyte membrane fuel cell *Nanotechnology* **15** S596
[22] Momma K and Izumi F 2011 VESTA 3 for three-dimensional visualization of crystal, volumetric and morphology data *J. Appl. Cryst.* **44** 1272
[23] Boyes E D, Ward M R, Lari L and Gai P L 2013 ESTEM imaging of single atoms under controlled temperature and gas environment conditions in catalyst reaction studies *Ann. Phys.* **525** 423
[24] Yoshida K, Zhang X, Bright A N, Saitoh K and Tanaka N 2013 Dynamic environmental transmission electron microscopy observation of platinum electrode catalyst deactivation in a proton-exchange-membrane fuel cell *Nanotechnology* **24** 065705
[25] Yoshida K, Bright A and Tanaka N 2012 Direct observation of the initial process of Ostwald ripening using spherical aberration-corrected transmission electron microscopy *J. Electron Microsc.* **61** 99
[26] Simonsen S B, Chorkendorff I, Dahl S, Skoglundh M, Sehesteda J and Helveg S 2011 Ostwald ripening in a PtsurasshuSiO2 model catalyst studied by *in situ* TEM *J. Catal.* **281** 147
[27] Zheng X, Mantzaras J and Bombach R 2014 Kinetic interactions between hydrogen and carbon monoxide oxidation over platinum *Combust. Flame* **161** 332
[28] Wulff G 1901 Velocity of growth and dissolution of crystal faces *Z. Kristallogr.* **34** 449
[29] Skriver H L and Rosengaard N M 1992 Surface energy and work function of elemental metals *Phys. Rev.* B **46** 7157
[30] Lopez N, Janssens T V W, Clausen B S, Xu Y, Mavrikakis M, Bligaard T and Nørskov J K 2004 On the origin of the catalytic activity of gold nanoparticles for low-temperature CO oxidation *J. Catal.* **223** 232
[31] Tomanek D and Mukherjee S 1983 Simple theory for the electronic and atomic structure of small clusters *Phys. Rev.* B **28** 665
[32] Kumar V and Kawazoe Y 2008 Evolution of atomic and electronic structure of Pt clusters: planar, layered, pyramidal, cage, cubic, and octahedral growth *Phys. Rev.* B **77** 205418
[33] Lopez-Haro M, Yoshida K, del Rio E, Perez-Omil J A, Boyes E D, Trasobares S, Zuo J M, Gai P L and Calvino J J 2016 Strain field in ultrasmall gold nanoparticles supported on cerium-based mixed oxides. Key influence of the support redox state *Lamgmuir* **32** 4313

[34] Hytch M J and Houdellier F 2007 Mapping stress and strain in nanostructures by high-resolution transmission electron microscopy *Microelectron. Eng.* **84** 460

[35] Nie A, Wu J, Zhou C, Yao S, Luo C, Forrey R C and Cheng H 2007 Structural evolution of subnano platinum clusters *Int. J. Quantum Chem.* **107** 219

[36] Walsh M J, Yoshida K, Kuwabara A, Pay M L, Gai P L and Boyes E D 2012 On the structural origin of the catalytic properties of inherently strained ultrasmall decahedral gold nanoparticles *Nano Lett.* **12** 2027

[37] Kinge S, Urgeghe C, De Battistib A and Bonnemann H 2008 Dependence of CO oxidation on Pt nanoparticle shape: a shape-selective approach to the synthesis of PEMFC catalysts *Appl. Organomet. Chem.* **22** 49

[38] Foiles S M, Baskes M I and Daw M S 1986 Embedded-atom-method functions for the fcc metals Cu, Ag, Au, Ni, Pd, Pt, and their alloys *Phys. Rev.* B **33** 7983

[39] Ferreira P J and Shao-Horn Y 2007 Formation mechanism of pt single-crystal nanoparticles in proton exchange membrane fuel cells *Electrochem. Solid-State Lett.* **10** 60

[40] Yoshida H, Kuwauchi Y, Jinschek J R, Sun K, Tanaka S, Kohyama M, Shimada S, Haruta M and Takeda S 2013 Visualizing gas molecules interacting with supported nanoparticulate catalysts at reaction conditions *Science* **335** 317